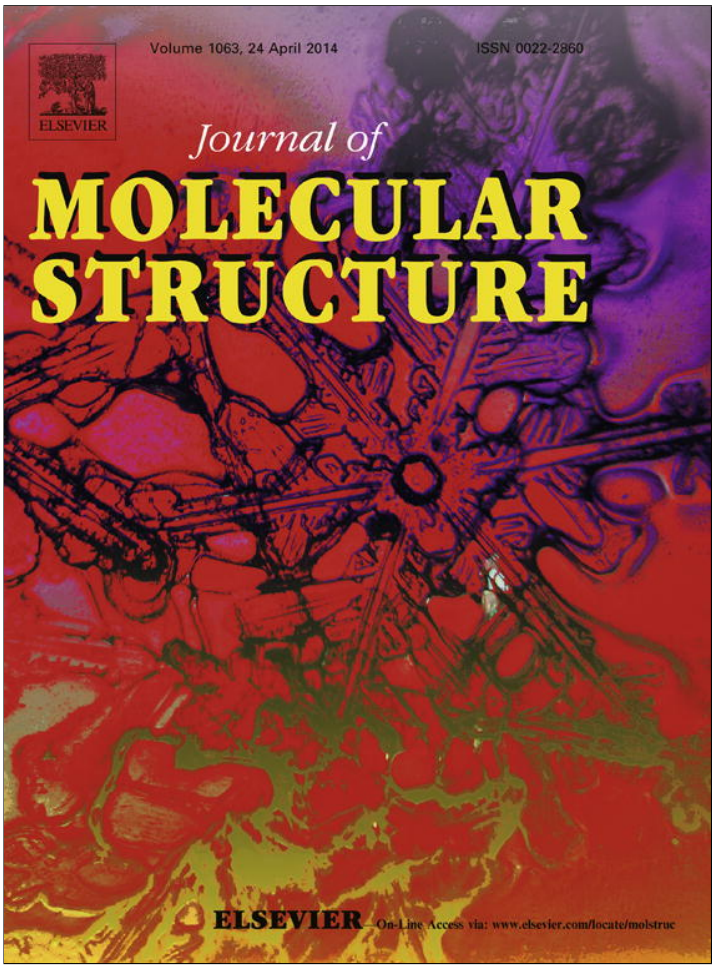

Journal of Molecular Structure 1063 (2014) 269–273

Contents lists available at ScienceDirect

Journal of Molecular Structure

journal homepage: www.elsevier.com/locate/molstruc

Structural and magnetic properties of $Ni_{1-x}Zn_xFe_2O_4$ nano-crystalline ferrites prepared via novel chitosan method

M.A. Gabal *, S. Kosa, T.S. Al Mutairi

Chemistry Department, Faculty of Science, King Abdulaziz University, Jeddah, Saudi Arabia

HIGHLIGHTS

- Zn-Substituted nickel ferrites were prepared via novel chitosan method.
- Effect of Zn-substitution on structural and magnetic properties was studied.
- An appropriate cation distribution was estimated using XRD and VSM techniques.

GRAPHICAL ABSTRACT

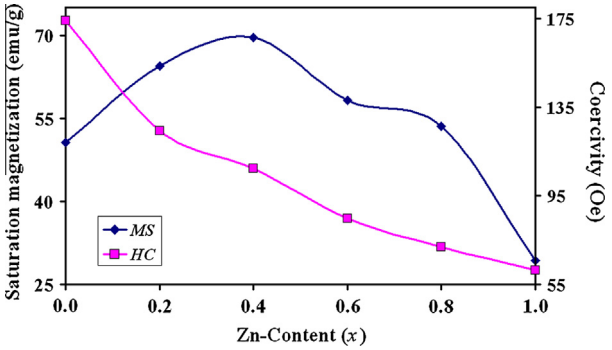

ARTICLE INFO

Article history:
Received 5 November 2013
Received in revised form 27 January 2014
Accepted 27 January 2014
Available online 1 February 2014

Keywords:
Chitosan method
Ni–Zn ferrites
XRD
Magnetic, cation distribution

ABSTRACT

In the present study, nano-crystalline $Ni_{1-x}Zn_xFe_2O_4$ ferrites ($x = 0.0–1.0$) were prepared via novel chitosan method. The prepared ferrites were characterized using X-ray diffraction (XRD), transmission electron microscopy (TEM), Fourier transform infrared spectroscopy (FT-IR) and vibrating sample magnetometer (VSM) techniques. XRD revealed the formation of spinel single-phase structure for the samples with Zn-content more than 0.4. The crystallite sizes estimated using Scherer formula are in the range 34–45 nm. TEM images reflect the agglomeration characteristics of the prepared ferrites. FT-IR spectra show two prominent characteristic peaks of ferrites. VSM measurement suggests the validity of the entire method for preparation of ferrites with high magnetization. The saturation magnetization was found to increase up to $x = 0.4$ then gradually decrease while coercivity decreased with increasing Zn-content. These changes in the magnetic properties by the addition of Zn were discussed depending on the estimated cation distribution of the system and the magneto-crystalline anisotropy of the entire ions, respectively.

1. Introduction

Synthesis and characterization of nano-crystalline ferrites have been attracted the attention of many investigators due to their enhanced optical, magnetic, and electrical properties, when compared with their bulk counterparts [1].

Nickel–zinc ferrites are soft magnetic materials having low coercivity and high electrical resistivity, which makes them an excellent core material for power transformer in electronic and telecommunication applications [2].

Nickel and zinc have strong occupational preference for tetrahedral and octahedral sites, respectively, which makes nickel ferrite a model inverse spinel and zinc ferrite a model normal one [3]. However, in Ni–Zn ferrites, the compositional variation can be resulted in the formation of mixed spinel structure, due to the redistribution of metal ions over the tetrahedral and octahedral sites,

* Corresponding author. Permanent address: Chemistry Department, Faculty of Science, Benha University, Benha, Egypt. Tel.: +966 557071572.
E-mail address: mgabalabdonada@yahoo.com (M.A. Gabal).

http://dx.doi.org/10.1016/j.molstruc.2014.01.070
0022-2860/

which can be drastically modified the ferrites properties [4,5]. On the other hand, the effect of preparation techniques on the cationic distribution and particles size cannot be neglected [6–8].

Slatineanu et al. [9] synthesized nano-crystalline $Ni_xZn_{1-x}Fe_2O_4$ via tartaric sol–gel auto-combustion method. The maximum value of the magnetization was found for $Ni_{0.8}Zn_{0.2}Fe_2O_4$ (63 emu/g).

Zhang et al. [10] prepared Ni–Zn ferrite nanoparticles using citrate combustion method. The lattice parameters were found to decrease with increasing Ni-content while coercivity increases.

Sarangi et al. [11] synthesized Ni–Zn ferrites by using oxalate precursor method. The magnetization, measured using vibrating sample magnetometer (VSM) lied between 34 and 49 emu/g depending on the composition.

Shahane et al. [3] prepared Ni–Zn ferrites through co-precipitation method. The magnetic measurements showed superparamagnetic nature for Ni-content up to 0.3, which changed to ferromagnetic one at higher Ni-content. The saturation magnetization was found to increase with increasing Ni-content.

Using X-ray diffraction and IR spectroscopy, Raghavender et al. [12] reported grain size decrease and lattice parameter increase with increasing Zn-content, for Ni–Zn ferrites prepared by citrate sol–gel method.

Yan et al. [13] synthesized Ni–Zn ferrites via solvothermal method. They reported that the maximum saturation magnetization, obtained using VSM, is for $Ni_{0.2}Zn_{0.8}Fe_2O_4$ (60.6 emu g^{-1}).

Shinde et al. [14] and Atif et al. [15] investigated the magnetic properties and cation distribution of Ni–Zn ferrites synthesized through oxalate co-precipitation method and sol–gel method. The saturation magnetization was found to increase up to Zn-content of 0.4 then decreases.

Gao et al. [16] studied the effect of composition and sintering temperature on the morphology and magnetic properties for a series of nano-structured $Ni_{1-x}Zn_xFe_2O_4$ (x = 0, 0.5 and 1) synthesized via sol–gel method. The highest saturation magnetization (70 emu/g) was obtained for $NiFe_2O_4$ calcined at 1073 K.

Sharma and Singhal [17] investigated the effect of Zn doping on the structural and magnetic properties of $Ni_{1-x}Zn_xFe_2O_4$ (x = 0.0–1.0) synthesized using sol–gel process. The saturation magnetization was found to increase up to x = 0.4 then decreases, while coercivity continuously decreasing.

Gabal et al. [6] prepared Ni–Zn ferrites using egg-white precursor method and suggested an appropriate cation distribution based on the obtained structural data.

Priyadharsini et al. [8] used glycine combustion method for preparing nano-crystalline Ni–Zn ferrites. The observed values of magnetization are in the range from 4 to 26 emu/g which is lower than that of bulk particles.

Really, it is clear from all the above that, more extensive works have to be carried out on Ni–Zn ferrites to meet the desired applications in different electronic devices. This is principally can be accomplished by either varying the chemical compositions or making appropriate changes in the processing procedures.

In the present work, our main goal is to prepare Ni–Zn ferrites nanoparticles via an alternative simple chitosan template route [18,19]. To the best of our knowledge, no report for preparing Ni–Zn ferrites via this route is present in the literature. It is of further interest to study the effect of non-magnetic Zn^{2+} ion substitution on the structural and magnetic properties of the entire system.

2. Experimental

2.1. Synthesis of $Ni_{1-x}Zn_xFe_2O_4$

Chitosan was used as a template [18,19] for the preparation of Nano-crystalline $Ni_{1-x}Zn_xFe_2O_4$ ferrites (x = 0.0–1.0). Stoichiometric amounts of the respective metal nitrates were weighed and dissolved in 100 mL distilled water. 1.6 g of chitosan was dissolved in 100 mL of acetic acid (3%, v/v) and added drop wisely under stirring to the nitrates solution. The temperature was then raised to 60 °C and after 30 min. NH_4OH solution (50%, v/v) was added drop wisely up to pH of 8. The gel formed was evaporated and kept on the hot plate until self-combustion. The obtained powders were taken the name; as-prepared chitosan precursors.

2.2. Techniques

Thermal decomposition of the gel precursor was characterized using a Perkin Elmer thermal analyzer. DTA–TG–DSC thermogram was monitored in air up to 600 °C at a heating rate of 5 K min^{-1}.

FT-IR spectra were recorded using a Perkin Elmer spectrophotometer in the range 4000–400 cm^{-1}.

X-Ray diffraction patterns were obtained using a Bruker D8 Advance X-ray diffractometer with Cu Kα radiation.

TEM image was recorded using JEOL 2010 Transmission Electron Microscope (TEM), operated at 100 kV.

Hysteresis loops were measured using Vibrating sample magnetometer (VSM-9600M) at room temperature with maximum applied field up to 10 kOe.

3. Results and discussion

3.1. Complexation mechanism and ferrite formation

Chitosan is a linear non-starch polysaccharide biopolymer composed of randomly distributed β-(1-4)-linked D-glucosamine and N-acetyl-D-glucosamine [20,21]. The amino groups besides the hydroxyl groups are acting as a dentate for the metal ions thus, facilate their close proximity and increase the amenability for their efficient reaction and easy production of ferrites.

The chitosan is insoluble in aqueous solution and the solubility increases by increasing acidity through the addition of acetic acid. When mixed with metals nitrates, the pH of solution must be increased up to about 8, by the addition of ammonia, so that the negatively charged amino and hydroxyl groups can be bounded with the metal ions and consequently forming gel.

Upon heating this gel in the presence of nitrates, an auto combustion reaction can be initiated in which the chitosan moiety acts as a fuel and the nitrates behave as an oxidant [22]. This exothermic reaction can be resulted in the decomposition of the organic matter into CO_2 and NO_x with the formation of ferrites nanoparticles.

This auto-combustion reaction can be followed through studying the thermal decomposition behavior of the gel precursor using DTA–TG measurements. Fig. 1 demonstrates a typical decomposition behavior in air of the gel-precursor with x = 0. The TG curve exhibits a total weight loss of 87.5% at 220 °C. The weight loss occurred between 30 and 180 °C, accompanied by small broad endothermic DTA peak, could be attributed the dehydration reaction. The major weight loss of 52.5% observed, which is characterized by a vigorous exothermic DTA peak at 210 °C, can be assigned to the auto-combustion reaction between nitrates oxidants and chitosan fuel, resulted in the evolution of water, CO_2 and NO_x with the formation of the respective ferrite. The absence of any thermal changes beyond 220 °C suggests the complete decomposition of any carbonaceous content.

3.2. Structural studies

3.2.1. X-ray diffraction

X-ray diffraction investigations (Fig. 2) indicated single-phase cubic structure for the as-prepared precursors except for the

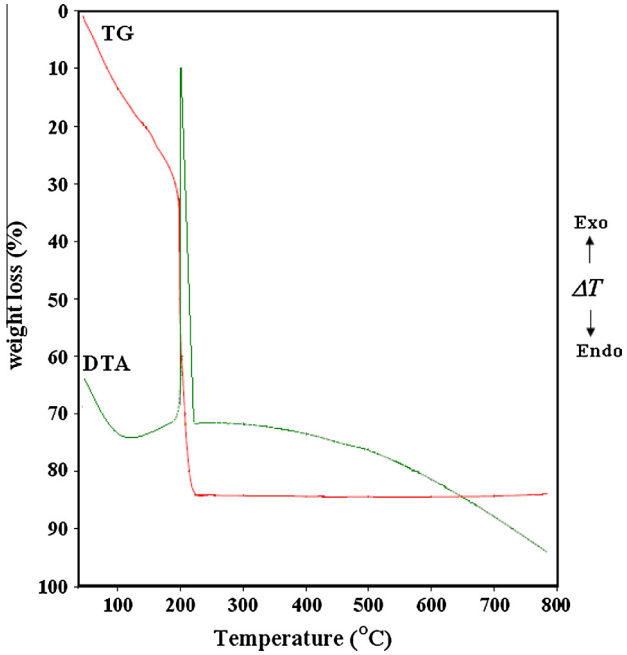

Fig. 1. DTA–TG curves in air of gel-precursor with $x = 0.0$. Heating rate = 5 °C min^{-1}.

samples with Zn-content ⩽0.4, which showed traces of Fe_2O_3. The increase in the lattice parameters (a_{exp}) with increasing Zn-content (Table 1) are attributed to the larger ionic radii of substituent Zn^{2+} ions compared to that of substituted Ni^{2+} ions [23] and agrees well with the reported data in the literature [6,17,24]. This increase in the lattice parameters by increasing Zn-content is accompanied by molecular weight increase (due to larger atomic weight of zinc compared with that of nickel) and thus, it is expected that it can give rise for nearly constant X-ray density (D_x) as appeared in Table 1. The obvious broadening of XRD peaks suggests the nano characteristics of the obtained powders. The average crystallite sizes (L) calculated using Scherer's equation [6] are listed in Table 1.

Based on the preferential occupancy of the entire cations [25] and taking into consideration the reported results on the effect of low temperature synthesis and nano-sized characteristics on the cation distribution of ferrites [4,5,26,27] an appropriate cation distribution for the entire system can be suggested. The estimated cation distributions along with their theoretically calculated lattice parameters (a_{th}) are presented in Table 1. The good agreement between the experimentally and theoretically calculated lattice parameters, suggests adequate cation distribution.

The inversion factor (γ) i.e. the number of iron atoms located in the tetrahedral site, oxygen lattice parameter (u), tetrahedral ionic radii (r_A), octahedral ionic radii (r_B), hopping length of A-sites (L_A) and B-sites (L_B) and intercationic distances were calculated [6] and reported in Table 1. The reported values could be easily discussed in the view of the estimated cation distributions and ionic radii of the entire ions. Sharma and Singhal have made similar calculations [17] on Zn-substituted $NiFe_2O_4$ synthesized via citrate sol–gel technique. The obvious difference between the results can be attributed to the difference between the cation distributions estimated in the two systems.

3.2.2. TEM images

Representative TEM of the entire ferrites with $x = 0.2$ and 0.8 are shown in Fig. 3. The images exhibit nano-sized particles with irregular shapes and sizes. The images also reflect the agglomeration characteristics of the prepared ferrites, which apparently appeared for the sample with Zn-content of 0.2 than that of 0.8. This agglomeration behavior suggests relatively high magnetic characteristics of the entire ferrites and can be raised due to the experience of nanoparticles for a permanent magnetic moment proportional to their volume [6].

3.2.3. FT-IR spectroscopy

Fig. 4 showed FT-IR spectra of the as-prepared precursors. The two characteristic bands appeared confirmed the formation of ferrospinels. These two bands can be assigned, according to Waldron [28], to the stretching vibration of metal oxygen bonds in tetrahedral and octahedral sites of the ferrite lattice. The frequency of the two bands, for different Zn-content, is summarized in Table 2. According to the band intensity, the higher frequency band can be due to the tetrahedral vibration while, the other one to the octahedral vibration. Similar results, for Zn-substituted $NiFe_2O_4$,

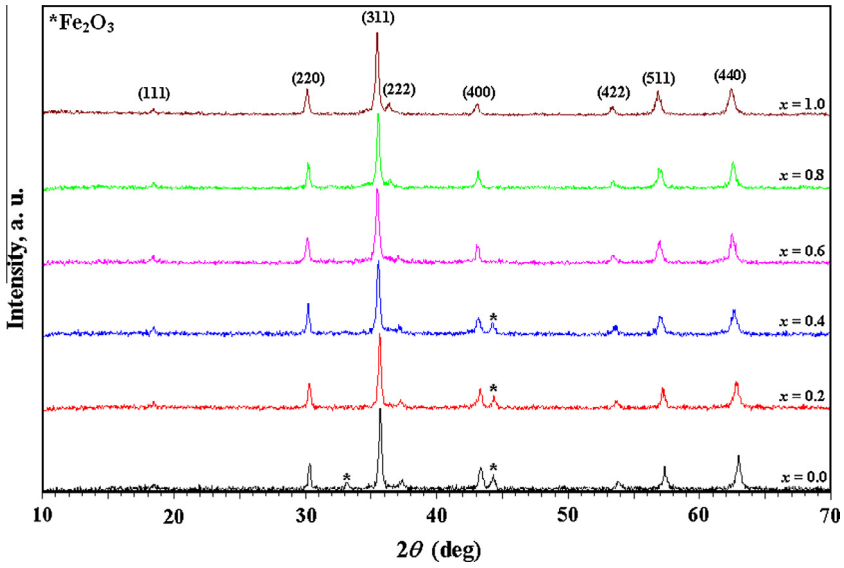

Fig. 2. XRD patterns of the as-prepared precursors.

Table 1
Structural data of $Ni_{1-x}Zn_xFe_2O_4$ system prepared using chitosan method.

Cation distribution (x)	a (Å)		r (Å)		L (nm)	D_X (g cm^{-3})	γ	u (Å)	L_A (Å)	L_B (Å)	Tet. bond	Oct. bond	Tet. edge	Oct. edge (Å)	
	a_{exp}	a_{th}	r_A	r_B										Shared	Unshared
(Fe)[NiFe]O_4	8.3395 ± 0.004	8.3390	0.490	0.667	44 ± 14	5.37	1	0.379	3.609	2.947	1.870	2.047	3.053	2.841	2.948
$(Fe_{0.8}Zn_{0.2})[Fe_{1.2}Ni_{0.8}]O_4$	8.3583 ± 0.007	8.3609	0.512	0.663	45 ± 13	5.38	0.8	0.380	3.615	2.952	1.891	2.040	3.089	2.815	2.953
$(Fe_{0.6}Zn_{0.4})[Fe_{1.4}Ni_{0.6}]O_4$	8.3831 ± 0.009	8.3827	0.534	0.659	40 ± 15	5.36	0.6	0.381	3.626	2.960	1.914	2.036	3.125	2.795	2.962
$(Fe_{0.6}Zn_{0.4})[Fe_{1.4}Ni_{0.4}Zn_{0.2}]O_4$	8.3942 ± 0.005	8.3961	0.534	0.663	34 ± 8	5.36	0.6	0.381	3.635	2.966	1.914	2.042	3.125	2.806	2.968
$(Fe_{0.6}Zn_{0.4})[Fe_{1.4}Ni_{0.2}Zn_{0.4}]O_4$	8.3903 ± 0.010	8.4095	0.534	0.669	37 ± 19	5.39	0.6	0.381	3.633	2.966	1.914	2.042	3.125	2.807	2.968
$(Fe_{0.6}Zn_{0.4})[Fe_{1.4}Zn_{0.6}]O_4$	8.4067 ± 0.007	8.4228	0.534	0.673	42 ± 10	5.39	0.6	0.381	3.640	2.972	1.914	2.048	3.125	2.818	2.974

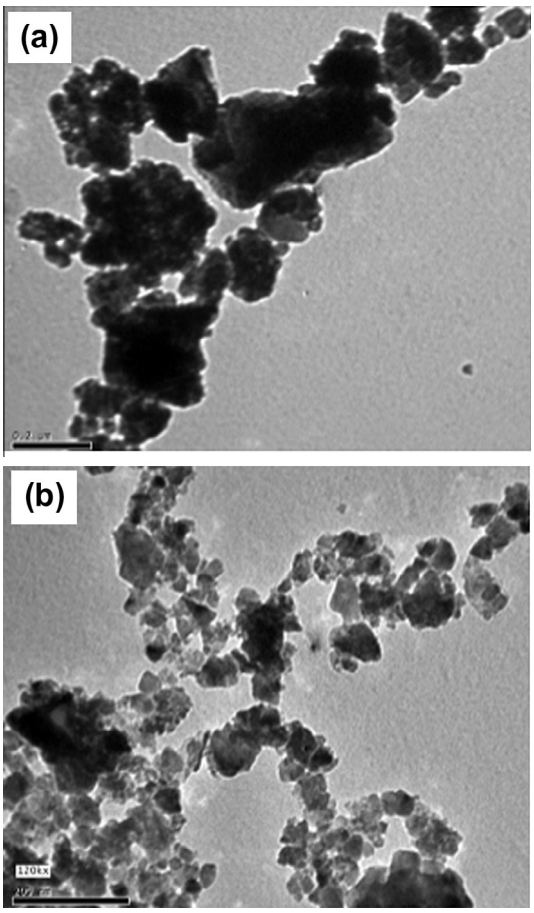

Fig. 3. TEM images of system: (a) $x = 0.2$ and (b) $x = 0.8$. (Scale bar: 200 nm.)

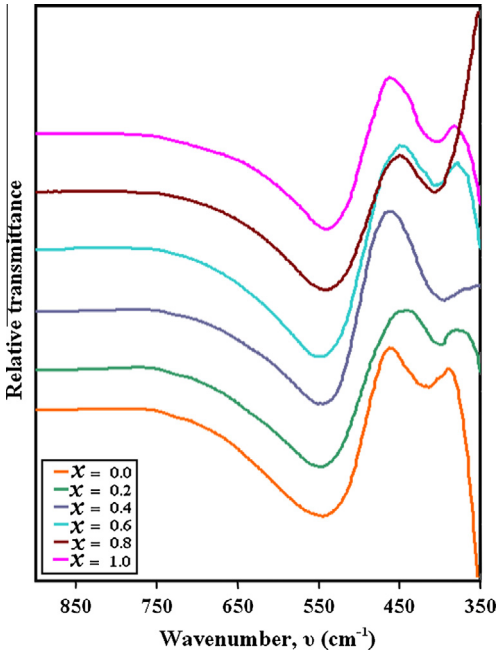

Fig. 4. FT-IR spectra of $Ni_{1-x}Zn_xFe_2O_4$ system.

Table 2
FT-IR spectral data and magnetic parameters of $Ni_{1-x}Zn_xFe_2O_4$ system.

x	ν_1, (cm^{-1})	ν_2 (cm^{-1})	Hysteresis loop				$\eta_B(x)$
			M_S	M_r	H_C	η_B	
0.0	555	413	50.6	11.9	174	2.1	2.3
0.2	548	398	64.4	10.7	124	2.7	3.8
0.4	545	395	69.6	11.2	107	3.0	5.4
0.6	545	406	58.2	8.3	85	2.5	4.9
0.8	541	407	53.6	6.9	72	2.3	4.5
1.0	541	402	29.3	4.3	62	1.3	4.0

synthesized using other methods, are reported in the literature [17,24].

3.3. Magnetic characteristics

The hysteresis loops measured at room temperature for the entire ferrites (Fig. 5) explain the ferromagnetic nature of the system. The values of saturation magnetization (M_S), coercivity (H_C) and retentivity (M_r) are reported in Table 2. The experimental magnetic moment (η_B) was determined from the saturation magnetization while, the calculated values ($\eta_B(x)$) are estimated from the suggested cation distribution [6].

Fig. 6 illustrates the effect of zinc substitution on saturation magnetization (M_S) and coercivity (H_C) from which it is clear that saturation magnetization increases up to $x = 0.4$ then gradually decreases while coercivity gradually decreases with increasing Zn-content. This magnetization behavior is in consistent with the reported results for Ni–Zn ferrites prepared through oxalate coprecipitation [14], sol–gel [17] and ceramic [29] methods. The high magnetization obtained indicates the validity of the entire chitosan method for the preparation of ferrites at relatively lower processing temperature (room temperature) and shorter duration. On the other hand, the lower magnetization values compared with that of the bulk samples [30], can be attributed to the finite size effects [31].

According to the estimated cation distribution (Table 1), and taking the values of magnetic moment of Fe^{3+}, Ni^{2+} and Zn^{2+} ions as 5, 2, and 0 μ_B, respectively [14] the theoretical magnetic moment $\eta_B(x)$ can be calculated assuming the Néel's two sublattices model of ferrimagnetism [32]. The obtained results (Table 2) describe well the magnetization behavior as follow: in $NiFe_2O_4$, Ni^{2+} ions preferably occupy the B-sites while, Fe^{3+} ions equally

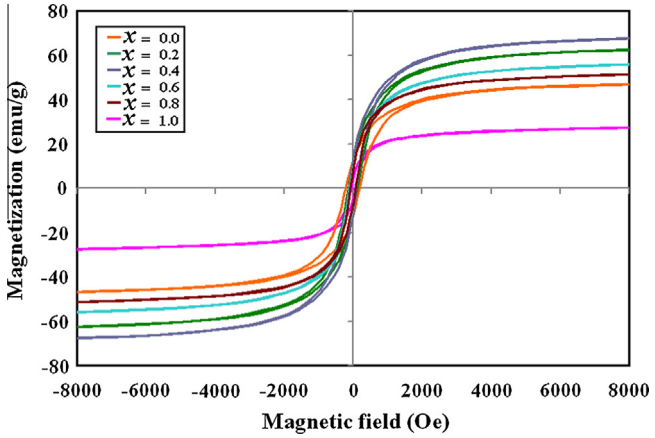

Fig. 5. Magnetic hysteresis loops for $Ni_{1-x}Zn_xFe_2O_4$ system.

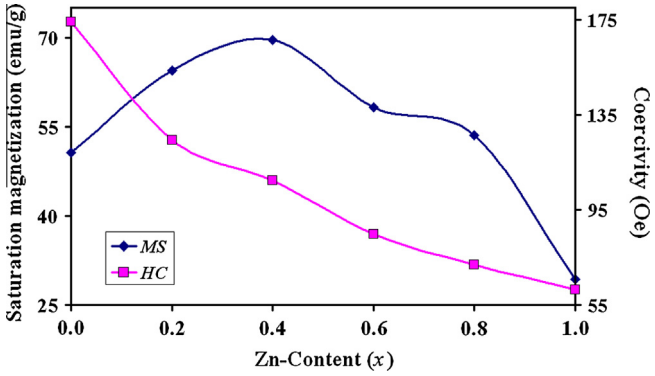

Fig. 6. Variation of the saturation magnetization and coercivity with x in $Ni_{1-x}Zn_xFe_2O_4$ system.

distributed among A- and B-sites. The introduction of non-magnetic Zn^{2+} ions will result in the migration of Fe^{3+} ions from A to B-sites, which will increase the magnetic moment of B-sites and consequently increases magnetization. This behavior lasts up to $x = 0.4$ after which, the excess Zn^{2+} ions tend to occupy B-sites. This abnormal substitution decreases the magnetic moment of B-sites and gradually results in decreasing magnetization.

The behavior of the experimental magnetic moment (η_B) agrees well with that theoretically calculated (Table 2) and the obvious difference between the two values suggested non-colinear spin arrangement [33].

The gradual decrease in the coercivity values with increasing Zn-content can be due to the lower magneto-crystalline anisotropy of zinc ferrite compared to that of nickel ferrite [10].

4. Conclusions

Nano-crystalline Ni–Zn ferrites were successfully synthesized using novel chitosan method. DTA–TG measurements revealed the ease of ferrites formation through the auto-combustion reaction. XRD indicated the formation of cubic spinels with average crystallite sizes in the range 37–45 nm. The gradual increase in the lattice parameters with the addition of Zn is attributed to the larger ionic radii of zinc compared to that of nickel. VSM measurements exhibit an increase in saturation magnetization up to $x = 0.4$ followed by a gradual decrease with increasing Zn-content. this behavior was described based on the suggested cation distribution of the entire ions. The coercivity showed a decrease behavior with the addition of Zn due to the difference in the magneto-crystalline anisotropy of ions. The relatively higher magnetization values obtained suggests the validity of the chitosan method for the preparation of ferrites with improved magnetic properties.

Acknowledgements

The Authors are grateful to Deanship of Scientific Research (DSR), King Abdulaziz University, Jeddah for providing financial support for this work. Also, the authors would like to express their thanks to Dr. Sharief, Chemistry Department, Benha University for his help and cooperation. Thanks extended also to Prof. R. El-Shishtawy for useful discussion.

References

[1] S.F. Neues, M.W.E. van den Berg, W. Grunert, L. Khodeir, J. Am. Chem. Soc. 127 (2005) 12028.
[2] A. Fawzi, A.D. Sheikh, V.L. Mathe, J. Alloys Compd. 502 (2010) 231.
[3] G.S. Shahane, A. Kumar, M. Arora, R.P. Pant, K. Lal, J. Magn. Magn. Mater. 322 (2010) 1015.
[4] H. Kavas, A. Baykal, M.S. Toprak, Y. Kseoglu, M. Sertkol, B. Aktas, J. Alloys Compd. 479 (2009) 49.
[5] C. Yao, Q. Zeng, G.F. Goya, T. Torres, J. Liu, H. Wu, M. Ge, Y. Zeng, Y. Wang, J.Z. Jiang, J. Phys. Chem. C 111 (2007) 12274.
[6] M.A. Gabal, R.M. El-Shishtawy, Y.M. AlAngari, J. Magn. Magn. Mater. 324 (2012) 2258.
[7] M.A. Gabal, Y.M. Al Angari, Mater. Chem. Phys. 115 (2009) 578.
[8] P. Priyadharsini, A. Pradeep, G. Chandrasekaran, J. Magn. Magn. Mater. 321 (2009) 1898.
[9] T. Slatineanu, A.R. Iordan, M.N. Palamaru, O.F. Caltun, V. Gafton, L. Leontie, Mater. Res. Bull. 46 (2011) 1455.
[10] H.E. Zhang, B.F. Zhang, G.F. Wang, X.H. Dong, Y. Gao, J. Magn. Magn. Mater. 312 (2007) 126.
[11] P.P. Sarangi, S.R. Vadera, M.K. Patra, N.N. Ghosh, Powder Technol. 203 (2010) 348.
[12] A.T. Raghavender, N. Biliskov, Z. Skoko, Mater. Lett. 65 (2011) 677.
[13] W. Yan, W. Jiang, Q. Zhang, Y. Li, H. Wang, Mater. Sci. Eng., B 171 (2010) 144.
[14] T.J. Shinde, A.B. Gadkari, P.N. Vasambekar, J Magn. Magn. Mater. 333 (2013) 152.
[15] M. Atif, M. Nadeem, R. Grssinger, R. Sato Turtelli, J. Alloys Compd. 509 (2011) 5720.
[16] P. Gao, X. Hua, V. Degirmenci, D. Rooney, M. Khraisheh, R. Pollard, R.M. Bowman, E.V. Rebrov, J. Magn. Magn. Mater. 348 (2013) 44.
[17] R. Sharma, S. Singhal, Physica B 414 (2013) 83.
[18] A. El Kadib, K. Molvinger, T. Cacciaguerra, M. Bousmina, D. Brunel, Micropor. Mesopor. Mater. 142 (2011) 301.
[19] A.B. Sifontes, G. Gonzalez, J.L. Ochoa, L.M. Tovar, T. Zoltan, E. Canizales, Mater. Res. Bull. 46 (2011) 1794.
[20] J. Nakamatsu, F.G. Torres, O.P. Troncoso, Y. Min-Lin, A.R. Boccaccini, Biomacromolecules 7 (2006) 3345.
[21] W.A. Morais, A.L.P. de Almeida, M.R. Pereira, J.L.C. Fonseca, Equilibrium, Carbohydr. Res. 343 (2008) 2489.
[22] C.C. Hwang, J.S. Tsai, T.H. Huang, Mater. Chem. Phys. 93 (2005) 330.
[23] R.D. Shannon, Acta Crystal. A 32 (1976) 751.
[24] S.M. Chavan, M.K. Babrekar, S.S. More, K.M. Jadhav, J. Alloys Compd. 507 (2010) 21–25.
[25] A. Goldman, Modern Ferrite Technology, second ed., Springer, New York, 2006.
[26] H. Kavas, A. Baykal, M.S. Toprak, Y. Kseoglua, M. Sertkol, B. Aktas, J. Alloys Compd. 479 (2009) 49.
[27] S. Bid, S.K. Pradhan, Mater. Chem. Phys. 82 (2003) 27.
[28] R.D. Waldron, Phys. Rev. 99 (1955) 1727.
[29] M. Ajmal, A. Maqsood, Mater. Lett. 62 (2008) 2077.
[30] R. Swaminathan, M.E. Mc Henry, P. Poddar, H. Srikanth, J. Appl. Phys. 97 (2005) 10G104.
[31] C.K. Kim, J.H. Lee, S. Katoh, R. Murakami, M. Yoshimura, Mater. Res. Bull. 36 (2001) 2241.
[32] L. Neel, Ann. Phys. 3 (1948) 137.
[33] S.M. Patange, S.E. Shirsath, B.G. Toksha, S.S. Jadhav, K.M. Jadhav, J. Appl. Phys. 106 (2009) 023914.